ELSEVIER

Physica B 283 (2000) 97–102

PHYSICA B

www.elsevier.com/locate/physb

Morphology of nanocermet thin films: X-ray scattering study

S. Hazra[a,*], A. Gibaud[a], A. Désert[a], C. Sella[b], A. Naudon[c]

[a]*Laboratoire de Physique de l'Etat Condensé, UPRESA 6087 CNRS, Faculté des Sciences, Université du Maine, 72085 Le Mans, France*
[b]*Laboratoire d'Optique des Solides, Université de Paris VI, 75006 Paris, France*
[c]*Laboratoire de Métallurgie Physique, Université de Poitiers, Poitiers, France*

Abstract

The morphology of ceramic–metal (cermet) thin films is studied by surface-sensitive X-ray scattering techniques. Grazing incidence small angle X-ray scattering (GISAXS) experiments carried out at LURE with a 2D detector show that metal clusters of nanometer size, known as nanoparticles, are dispersed in the thin film. Analyses of the X-ray reflectivity along with the diffuse scattering allow to predict the formation of layers of nanoparticles along the growth direction of the films. The formation of such cumulative-disordered layers in one direction is likely to be related to the boundary condition in the reduced dimension. © 2000 Elsevier Science B.V. All rights reserved.

Keywords: X-ray scattering; Thin film morphology; Nanoparticles; Ceramic metals

1. Introduction

Small clusters of metallic atoms, known as nanoparticles, are gaining importance for the diverse technical applications arising from the fundamental physics such as quantum size effects [1,2]. In nanoparticles, the large surface to volume ratio finds important applications in heterogeneous catalysis, heat exchangers and thermometers at ultra-low temperatures and magnetic devices [3]. However, the study of independent nanoparticles is not very easy due to their high reactivity. This can be overcome by coating the particles with some polymer or insulating medium. One can also think of thin films, in which metal nanoparticles are dispersed in an insulating ceramic matrix (cermets). Technologically, cermets have been used in solar energy plants to absorb radiation in the visible and infra-red regions of the solar spectrum [4]. The absorption of radiation depends on the concentration and nature of the metallic particles in the cermet films. So far, their optical properties have been presented in detail from an experimental point of view but interestingly their morphology is not really understood. The morphology is, however, important to predict the different interesting physical properties of that system.

Recently, surface sensitive X-ray and neutron scattering became extremely powerful techniques to study the morphology of the thin films in a nondestructive way. Specular reflectivity, in particular, gives the scattering density profile in the direction normal to the surface of a thin film from which one can get the average film thickness, interfacial roughness and the average position of the materials along that growth direction [5,6]. Diffuse scattering, on the other hand, is helpful to extract information about the in-plane correlation of interfacial roughness [7–9] or composition in thin films. Combination of specular reflectivity and diffuse scattering have been extensively carried out to determine the structure of, especially, homogeneous monolayer and multilayered thin films [10–14]. Up to now less work has been done to study the morphology of heterogeneous (like nanocermet) thin films [15–18]. The study of heterogeneous medium such as surfactant dispersed in some solution has been carried out mostly through small angle scattering (SAS) in transmission geometry to find out the shape, size, separation and interaction of the surfactants in the solution [19]. Conventional SAS technique cannot be used directly in case of thin films due to the presence of the substrate and to the small amount of scattering material. This has recently been overcome by measuring

* Corresponding author.
E-mail address: shazra@aviion.univ-lemans.fr (S. Hazra)

0921-4526/00/$ - see front matter © 2000 Elsevier Science B.V. All rights reserved.
PII: S0921-4526(99)01899-2

the X-ray scattering at grazing incidence angle (GISAXS) from thin films in reflection geometry [20].

In this contribution we present the morphology of three nanocermet thin films using such surface sensitive X-ray scattering techniques.

2. Experiment

Cermet films of Pt-Al_2O_3 were made by co-sputtering the amorphous Al_2O_3 with the metallic Pt on float glass substrates. Three samples (PAG4, PAG8 and PAG12) prepared for different durations of time, keeping all other parameters fixed, are presented here.

X-ray specular reflectivity and longitudinal and transverse diffuse scattering (called in the following conventional geometry) were performed using a laboratory source (Philips diffractometer) of wavelength 1.54 Å. GISAXS measurements of the samples were performed using synchrotron source (D22 beam line, LURE) at energy 7 keV. All measurements were performed in reflection geometry, as shown in Fig. 1. The surface of the sample is located in the x–y plane and the incident X-ray beam is in the x–z plane. α is the incident angle with the x–y plane and β and ϕ are the exit angles with the x–y and x-z planes, respectively. The components of the wave vector transfer, $\boldsymbol{q}$ (q_x, q_y, q_z), corresponding to the incident wavelength λ are $q_x = (2\pi/\lambda)(\cos\beta\cos\phi - \cos\alpha)$, $q_y = (2\pi/\lambda)(\cos\beta\sin\phi)$, $q_z = (2\pi/\lambda)(\sin\alpha + \sin\beta)$. All measurements made with the lab source were carried out at $\phi = 0$ yielding $q_x = (2\pi/\lambda)(\cos\beta - \cos\alpha)$ and $q_y = 0$. For specular measurements $\alpha = \beta = \theta$, so that $q_x = 0$ and $q_z = (4\pi/\lambda)(\sin\theta)$. For transverse diffuse scattering measurements, the scattering angle $\alpha + \beta = 2\theta$ was maintained at a fixed value. The synchrotron measurements were carried out at a fixed incidence angle, $\alpha \sim 0.45^\circ$ (slightly greater than the critical angle, α_c, of the film), using a two-dimensional (2D) detector fixed in y–z plane. The specular reflectivity was masked to avoid the saturation of the detector. It is interesting to comment on the difference between the two sets of measurements. Firstly, in conventional geometry, scans are measured with a varying incident angle whereas GISAXS measurements are performed at fixed incident angle. In GISAXS measurements the illuminated area is therefore constant and the penetration depth depends on the chosen incidence. Secondly, in GISAXS measurements, the specular reflectivity is not measured and the diffuse scattering is collected over a very large area in reciprocal space which mainly depends on the sample to detector distance. This gives the possibility to measure very short correlation lengths (typically $\xi < 100$ Å) and more importantly the anisotropy of the scattering is determined. This is extremely useful to get information about the way nanoparticles are located in the thin film. In conventional geometry, the measurement of diffuse scattering is only valid up to the location of the Yoneda wings. As they are usually found around $q_x < 5 \times 10^{-3}$ Å^{-1}, the analysis of diffuse scattering in this geometry usually gives access to large correlation lengths (10 μm $> \xi >$ 100 Å). The two sets of measurements are therefore very complementary in the sense that conventional measurements give information about the morphology in the direction normal to the surface and about large correlated features in the plane of the interfaces and GISAXS measurements probe small correlation lengths anywhere except in the specular direction.

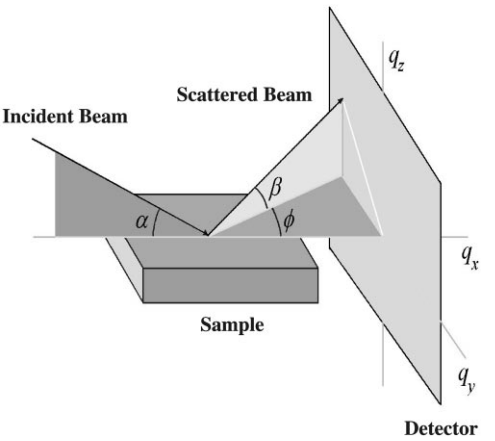

Fig. 1. Schematic of the scattering geometry used to perform X-ray measurements. Details are given in the text.

3. Results and discussion

Reciprocal space maps of the films obtained from GISAXS measurements are shown in Fig. 2. All the images show the presence of a highly intense region close to the centre followed by a nearly elliptical ring. The intensity collected close to the centre corresponds to the scattering near the critical angle of total external reflection and will be ignored in the following. The intense annular ring can be considered as the scattering from Pt clusters present in the films. The distance of the ring from the origin is related to the average separation of the cluster particles in a particular direction. The shape of the ring is related to the shape, size and distribution of the particles in the films. Since the ring is elliptical it means that the average separation between particles along z is greater than that along x–y plane. Similarly the shape being almost identical in any direction indicates that the particles are nearly spherical. One can also clearly observe that the intensity of the ring increases with the thickness of the samples.

The specular X-ray reflectivity and longitudinal off-specular (off-set 0.12°) scattering are shown in Fig. 3. All

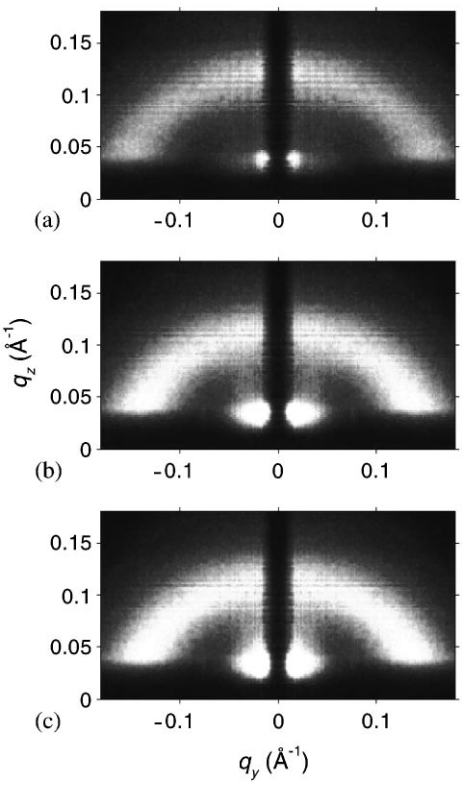

Fig. 2. GISAXS images at a fixed incidence angle of the three nanocermet thin films: (a) PAG4, (b) PAG8 and (c) PAG12.

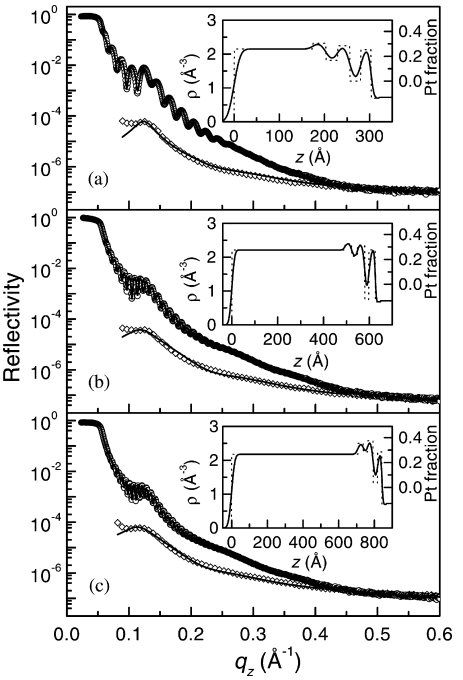

Fig. 3. Reflectivity (○) and longitudinal diffuse scattering (◇) data of the three nanocermet thin films in three different panels: (a) PAG4, (b) PAG8 and (c) PAG12. Solid lines passing through the reflectivity data are the best fit curves obtained for the EDP shown in the inset of each panel. Solid lines passing through the diffuse scattering data are the calculated curves using Eq. (4) for the same set of parameters as for Fig. 5.

the reflectivity curves follow the same behaviour: for $q_z < 0.054$ Å^{-1}, the reflectivity is nearly one due to total external reflection; near $q_z \sim 0.054$ Å^{-1}, there is a rounding of the reflectivity curve due to the high absorption, followed by a sharp decrease due to the surface roughness; for $q_z > 0.054$ Å^{-1}, there are oscillations, known as Kiessig fringes which are due to the total film thickness. The separation between consecutive fringes is inversely proportional to the film thickness. A broad hump around $q_z \sim 0.124$ Å^{-1} is observed in all reflectivity curves. A similar hump is also observed in each of the off-specular scattering curve. However, its intensity is about two orders of magnitude less compared than that of the specular one. The transverse diffuse scattering data around two specular positions ($q_z = 0.124$ and 0.25 Å^{-1}) for the three films are shown in Fig. 4. All the transverse curves show the presence of a sharp specular central component dominating the low diffuse scattering. Diffuse scattering normalised to specular value is observed to increase with the film thickness.

The average critical wave vector (q_c) is related to the average electron density (ρ) of the film and from that one can extract the volume fraction of Pt in the film using simple relation

$$x = \frac{\rho_{\text{film}} - \rho_{\text{matrix}}}{\rho_{\text{Pt}} - \rho_{\text{matrix}}} = \frac{q_{\text{c, film}}^2 - q_{\text{c, matrix}}^2}{q_{\text{c, Pt}}^2 - q_{\text{c, matrix}}^2}. \quad (1)$$

The q_c for matrix (Al_2O_3) and Pt are 0.041 and 0.083 Å^{-1}, respectively. So the volume fraction of Pt for the present cermet films having average $q_c \sim 0.054$ Å^{-1} is 0.24.

In the kinematical approximation, the scattering intensity which is measured in the experiment is the square of the total scattering amplitude and can be written as

$$I(\boldsymbol{q}) = \left| \int \rho(\boldsymbol{r}) e^{-i\boldsymbol{q}\cdot\boldsymbol{r}} \, d\boldsymbol{r} \right|^2, \quad (2)$$

where $\rho(\boldsymbol{r})$ is the electron density of the film at position $\boldsymbol{r}$. For a heterogeneous thin film, where metal clusters are randomly distributed in the amorphous matrix, the above electron density can be written as [17,21,22]

$$\rho(\boldsymbol{r}) = \left[\rho_{\text{matrix}} + \Delta\rho \sum_i \delta(\boldsymbol{r} - \boldsymbol{r}_i) \otimes S_{\text{cluster}}(\boldsymbol{r}_i) \right] S_F(\boldsymbol{r}), \quad (3)$$

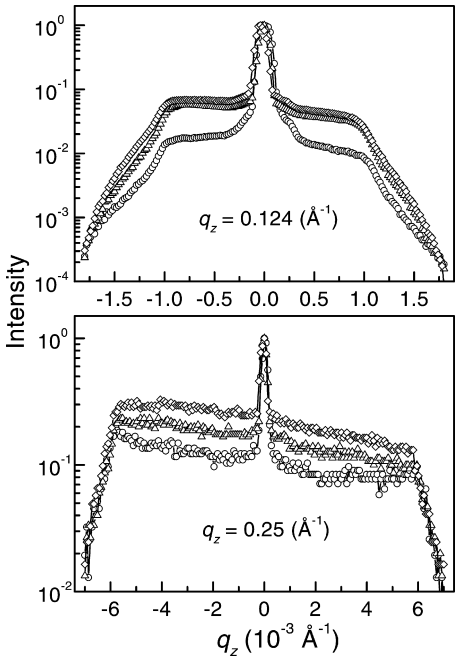

Fig. 4. Transverse diffuse scattering of the three ((○) PAG4, (△) PAG8; and (◇) PAG12) nanocermet thin films at two different q_z values.

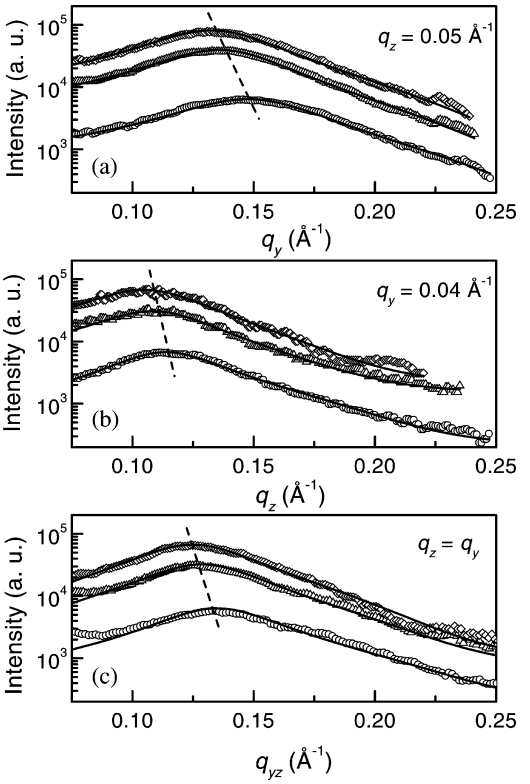

Fig. 5. Diffuse scattering along different directions obtained from GISAXS measurements of the three ((○) PAG4; (△) PAG8; and (◇) PAG12) nanocermet thin films: (a) along q_y for fixed q_z, (b) along q_z for fixed q_y and (c) along 45° with q_y and q_z. Solid lines are the calculated curves using Eq. (4) and corresponding parameters are listed in Table 1.

where $\Delta\rho = \rho_{\text{cluster}} - \rho_{\text{matrix}}$, $S_{\text{cluster}}(\boldsymbol{r}_i)$ is related to the shape and size of the ith cluster at a position $\boldsymbol{r}_i$ and $S_{\text{F}}(\boldsymbol{r})$ is related to the limited dimension of the film, which basically dictates the integration limit of Eq. (2). Considering the case of limited dimension, the scattered intensity can be split into two terms: one only along the specular direction and the other diffuse in all directions. If we consider that spherical clusters of radius R are distributed in the matrix according to the cumulative disorder having average separation d, then the diffuse part can be considered arising from the clusters as

$$I_{\text{cluster}} \propto \frac{(\sin qR - qR\cos qR)^2}{(qR)^6} \times \frac{1 - \mathrm{e}^{-2q^2\sigma_d^2}}{1 - 2\cos(qd)\mathrm{e}^{-q^2\sigma_d^2} + \mathrm{e}^{-2q^2\sigma_d^2}}, \quad (4)$$

where σ_d is the variance of d. In actual calculation one has to consider the variance of R as well. Eq. (4) has been derived considering spherical shape and the isotropic distribution of the particles and neglecting the limited dimensional effect of the film. Limited dimension along z of the film will modify the value of I_{cluster} especially in the specular direction and can be considered as same in all other directions. However, in practice this may not be the case if the distribution and/or shape of the particles are not spherically symmetric and one has to modify the equation accordingly. To have a clear look at this symmetric (or asymmetric) behaviour we have plotted line profiles in three different directions on the GISAXS images, as shown in Fig. 5. This figure shows clearly the increase of interparticle separation with the thickness and the larger separation along z compared to that along x–y plane. Considering different value of d (d_z and d_{xy}) as well as R (R_z and R_{xy}) along z and in-plane, respectively, we have calculated the scattering intensity using Eq. (4). The calculated intensity is shown in Fig. 5 and the parameters used for the calculation are listed in Table 1. Analysis shows that the separation of the particles along z is not only more than that along x–y plane but the size of the particles along z is slightly larger than that along x–y. This indicates that the shape of the particles is ellipsoidal with the elongation along the z-direction. It can be noted from the image and the results listed in Table 1 that the size and the separation of the particles are increasing slightly with the increase in the film thickness. Increase in the size of the metal particles was observed in metal thin film with growing time [23,24] which indicates the dynamical behaviour of the films. However,

Table 1
Parameters of the nanocermet thin films obtained from the analysis of the X-ray scattering measurements[a]

Sample	$2R_{xy}$ (Å)	$2R_z$ (Å)	d_{xy} (Å)	d_z (Å)	d_L (Å)	D (Å)	σ_t (Å)
PAG4	28.2 (3.0)	32.0 (6.5)	38.5 (8.0)	52 (12)	52	303	11.3
PAG8	31.0 (3.5)	34.8 (8.0)	42.0 (8.6)	52 (13)	54	625	13.7
PAG12	31.0 (3.5)	35.4 (8.0)	42.8 (9.0)	53 (14)	55	842	14.3

[a]*Note*: The variance of the parameters are given within parenthesis.

unlike simple metal thin film, the metal nanoparticles in cermet films probably cannot grow too much due to the presence of the insulating matrix. It is also interesting to note that the shape of the nanoparticles in metal thin films was found to be ellipsoidal with an elongation in the x–y direction due to the wetting/nonwetting properties of the metal with the substrate [24], while ellipsoidal particles elongated along z were found in these cermet thin films which may be due to the presence of the ceramic matrix.

Let us now concentrate on the specular direction. As mentioned above there is a broad hump around $0.124\ \text{Å}^{-1}$ (Fig. 3) which is close to the position of the annular ring observed in the q_z-direction in Fig. 2. We believe that the observation of this hump is related to presence of the metallic particles. However, since the transverse diffuse scattering (Fig. 4) is strongly peaked at the specular position, the particles must be arranged in such a way that the scattering from the particles is stronger for $q_x = q_y = 0$. This can only happen if we consider the formation of layering of particles along q_z. In that case, one can calculate the scattering along q_z, i.e. specular reflectivity by using the matrix technique in a similar way to what is done in a multilayer. In order to calculate the reflectivity we divide the films into slabs having different electron density. As a starting value, we consider the films having layers alternatively rich and poor in electron densities and the separation between two consecutive rich (or poor) layers is such that it gives rise to the hump (at $\sim 0.124\ \text{Å}^{-1}$) in the reflectivity curve. EDP obtained from the fitting of the reflectivity data is shown in the inset of Fig. 3. The total film thickness (D), the top surface roughness (σ_t) and the separation (d_L) between first and second layers of particles for all the three films obtained from the EDP are listed in Table 1. The x–y average compositional variation (Pt fraction) along z-direction of the films is also labeled in the inset of Fig. 3. For all the films the compositional profile shows strong variation in composition close to the substrate with almost constant composition in the top portion of the films. The variation in the compositional profile can be explained in terms of the formation of layering of particles. The growth of the film starts from the solid smooth substrate and such a boundary condition helps to form most of the first nanoparticles in a given x–y plane. This boundary condition is necessarily relaxed during the growth process since all the particles do not have exactly the same radius and the same interparticle separation. As the growth process continues the particles which are first well stacked in the z-direction become more and more disordered. The first layer close to the substrate is due to particles which have variation in the z-direction mainly due to the substrate roughness and which have some size and its variance. The location of the second layer with respect to the first one is mainly dictated by the average particle separation along the z-direction. The broadening of the layer can be attributed to the variance in separation. Variance in separation between the particles makes the x–y average z-position of the particles almost random after few (3–4) layers which in turn gives rise to a constant electron density.

4. Conclusion

We exploit surface sensitive X-ray scattering measurements to bring out the morphology of nanocermet thin films in a nondestructive way. Pt-Al_2O_3 cermet thin films of different thickness were deposited on glass substrates by co-sputtering Pt and Al_2O_3 for different durations of time. GISAXS of the films were carried out using synchrotron source, which shows that the films are made of ellipsoidal nanoparticles of Pt elongated slightly along z, distributed in the amorphous alumina matrix. The average separation of the particles along z is found to be more than that in the in-plane direction. Specular X-ray reflectivity and diffuse scattering of these films were also carried out using lab source shows the layering of particles along the growth (z) direction of the film. The layering of particles is prominent close to the substrate and decays gradually with the thickness of the film. Such layering of the particles close to the substarte is likely to be related to boundary condition of the substrate. The nucleation of the Pt starts from the substrate after co-sputtering of the materials, so the smooth substrate is likely to help to form all the particles in a x–y plane close to substrate. As the growth continues the formation of particles in the z-direction become random due to the relaxation of such a boundary condition. The size and separation of the particles is found to increase slightly

with the film thickness, which may be related to the dynamics of the growth process.

Acknowledgements

We are greatly indebted to the LURE facility for the measurements of GISAXS and particularly to O. Lyon.

References

[1] A.P. Alivisatos, Science 271 (1996) 933.
[2] J. Schi, S. Gider, D.D. Awschalom, Science 271 (1996) 937.
[3] W.P. Halperin, Rev. Mod. Phys. 58 (1986) 533.
[4] G.A. Niklasson, C.G. Grandqvist, J. Appl. Phys. 55 (1984) 3382.
[5] I.K. Robinson, D.J. Tweet, Rep. Prog. Phys. 55 (1992) 599.
[6] A. Gibaud, G. Vignaud, S.K. Sinha, Acta Crystallogr. A 49 (1993) 642.
[7] S.K. Sinha, E.B. Sirota, S. Garoff, H.B. Stanley, Phys. Rev. B 38 (1988) 2297.
[8] M.K. Sanyal, S.K. Sinha, K.G. Huang, B.M. Ocko, Phys. Rev. Lett. 66 (1991) 628.
[9] A. Gibaud, N. Cowlam, G. Vignaud, T. Richardson, Phys. Rev. Lett. 74 (1995) 3205.
[10] J. Daillant, O. Bélorgey, J. Chem. Phys. 97 (1992) 5824.
[11] V. Holy, J. Kubena, I. Ohidal, K. Lischka, W. Plotz, Phys. Rev. B 47 (1993) 15 896.
[12] J.P. Schlomka, M. Tolan, L. Schwalowsky, O.H. Seeck, J. Stettner, W. Press, Phys. Rev. B 51 (1995) 2311.
[13] T. Salditt, D. Lott, T.H. Metzger, J. Peisl, G. Vignaud, P. Hogho, O. Schärpf, P. Hinze, R. Lauer, Phys. Rev. B 54 (1996) 5860.
[14] J.K. Basu, S. Hazra, M.K. Sanyal, Phys. Rev. Lett. 82 (1999) 4675.
[15] J.R. Levine, J.B. Cohen, Y.W. Chung, P. Georgopoulos, J. Appl. Cryst. 22 (1989) 528.
[16] M. Rauscher, T. Salditt, H. Spohn, Phys. Rev. B 52 (1995) 16 855.
[17] M. Maaza, A. Gibaud, C. Sella, B. Pardo, F. Dunsteter, J. Corno, F. Bridou, G. Vignaud, A. Désert, A. Menelle, Eur. Phys. J. B 7 (1999) 339.
[18] B.A. Korgel, D. Fitzmaurice, Phys. Rev. B 59 (1999) 14 191.
[19] S.H. Chen, E.Y. Sheu, J. Kalus, H. Hoffmann, J. Appl. Crystallogr. 21 (1988) 751.
[20] A. Naudon, D. Babonneau, Z. Metallkd. 88 (1997) 596.
[21] B.K. Vainshtein, Diffraction of X-rays by Chain Molecules, Elsevier, Amsterdam, 1966.
[22] G. Vignaud, Thesis, 1997.
[23] H. You, K.G. Huang, R.T. Kampwirth, Physica B 221 (1996) 77.
[24] S. Kundu, S. Hazra, S. Banerjee, M.K. Sanyal, S.K. Mandal, S. Chaudhuri, A.K. Pal, J. Phys. D: Appl. Phys. 31 (1998) L73.